Revista Mexicana de Astronomía y Astrofísica, **48**, 199–207 (2012)

NEW ANALYTIC AND QUASI-ANALYTIC SOLUTIONS FOR WIND-DRIVEN COMPACT HII REGIONS

A. C. Raga,[1] J. Cantó,[2] and L. F. Rodríguez[3]

Received 2012 February 10; accepted 2012 April 3

RESUMEN

Las regiones HII ultracompactas están en un régimen de balance de presión aproximado con las nubes moleculares densas circundantes. En este artículo aplicamos un nuevo formalismo de "cáscara gruesa" al caso de una región HII energizada tanto por la fotoionización como por el viento de una estrella central. El modelo resultante lleva a soluciones analíticas y cuasi-analíticas que tienen una transición a un régimen (ausente en la solución analítica clásica de una burbuja alimentada por un viento) en el que la burbuja caliente alimentada por el viento se expande cuasi-estáticamente, en equilibrio de presión aproximado con el medio ambiente circundante. Este régimen es relevante para las regiones HII ultracompactas observadas. Presentamos la evolución temporal del radio y del ancho de la cáscara fotoionizada en expansión para distintos valores del parámetro adimensional que determina las características de la solución.

ABSTRACT

Ultracompact HII regions are in a regime of approximate pressure balance with the surrounding, dense molecular clouds. In this paper, we apply a newly developed "thick shell" formalism to the case of an expanding HII region energized by both the photoionizing radiation and the wind from the central stellar source. The resulting model leads to analytic and quasi-analytic solutions that have a transition to a regime (absent in the classical "wind-driven bubble" analytic solutions) in which the hot, stellar wind bubble expands quasi-statically, in approximate pressure equilibrium with the surrounding ISM. This regime is relevant for the observed ultracompact HII regions. We present the time-evolution of the radius and the thickness of the expanding HII shell for different values of a single, dimensionless parameter that determines the characteristics of the solution.

Key Words: HII regions — ISM: evolution — ISM: kinematics and dynamics — stars: formation

1. INTRODUCTION

The problem of the interaction of the stellar wind from a massive star and a homogeneous, surrounding ISM has been studied for several decades (see, e.g., Pikel'ner 1968; Dyson & de Vries 1972; Falle 1975; and the more recent work of García-Segura & Franco 1996). The relevance of this interaction in the context of expanding HII regions was apparently first discussed by Dyson (1977).

The relatively recent observations of ultracompact HII regions, with sizes as small as $\sim$0.03 pc, embedded in molecular clouds of densities of up to $\sim 10^7$ cm^{-3} (see, e.g., the review of Kurtz 2005) show that these objects have expanded to reach pressure equilibrium with the surrounding clouds (see, e.g., de Pree, Rodríguez, & Goss 1995; Franco et al. 2007). Motivated by these observations, Raga, Cantó, & Rodríguez (2012a) have developed a new "thick shell" model for the expansion of HII regions (in the absence of a stellar wind). This model leads to a full analytic solution which has the correct relaxation to the final state of pressure equilibrium between the photoionized region and the surrounding, neutral gas.

[1]Instituto de Ciencias Nucleares, Universidad Nacional Autónoma de México, Mexico.

[3]Instituto de Astronomía, Universidad Nacional Autónoma de México, Mexico.

[3]Centro de Radioastronomía y Astrofísica, Universidad Nacional Autónoma de México, Morelia, Michoacán, Mexico.

In the present paper, we apply this "thick shell" formalism to the case of an expanding HII region driven by both the ionizing radiation and a wind from the central star. The new formalism leads to expansion laws that differ from the "classical" solution (Dyson 1977), and which are relevant for the rapidly evolving ultracompact HII regions.

The paper is organized as follows. In § 2, we describe the general characteristics of the flow. In § 3, we develop a "thick shell" model in which the photoionized region is assumed to be thin (most of the width of the thick shell being filled with displaced, neutral environmental gas). In § 4, we remove the assumption of a thin photoionized region, and develop the corresponding model. Finally, in § 5 we discuss the possible applications of our models to observations of ultracompact HII regions.

2. THE FLOW CONFIGURATION

We assume that we have the flow configuration shown in Figure 1:

1. A star has an isotropic wind (of mass loss rate $\dot{M}$ and terminal velocity v_w) which is turned on at $t = 0$. At a time $t > 0$ the wind fills the inner, spherical region labeled "I" in the schematic diagram. The star also emits S_* photoionizing photons per unit time (starting at $t = 0$). The outer boundary of this region is a spherical shock, which has a radius much smaller than the ones of all of the other regions of the flow,

2. The shocked stellar wind produces a hot bubble of coronal gas (region II, which is non-radiative for the case of an O/B central star) limited on the outside by a contact discontinuity which separates the stellar wind from disturbed environmental material,

3. The hot bubble pushes out a shock wave (the outer boundary of region III in the schematic diagram) into the surrounding, neutral environment (region IV). The shell of displaced environmental material has an inner region (region IIIa) which is photoionized by the S_* ionizing photon rate of the central star, and a neutral outer region (region IIIb).

We first assume that region IIIa (the HII region) is much thinner than region IIIb (the region filled with shocked, neutral material, see Figure 1). For this "thin HII region" case, one can derive a model resulting in a first order differential equation with an approximate analytic solution. This model is described in § 3.

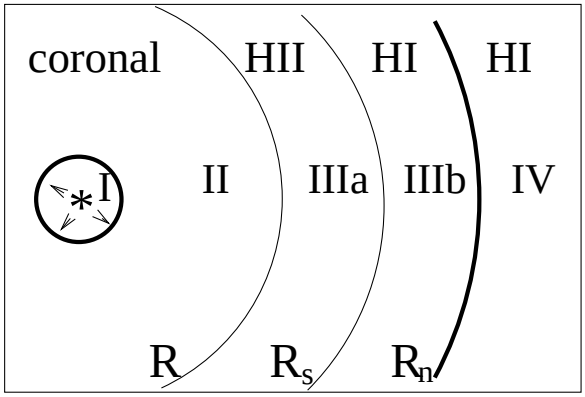

Fig. 1. Schematic diagram of a wind-driven HII region. The asterisk indicates the position of the ionizing photon+stellar wind source. Region I is filled with the expanding stellar wind, ending at an outer shock (thick, inner circle). Region II is filled with the hot, shocked wind, and ends in a contact discontinuity (at a radius R). Region IIIa is the photoionized region (of outer radius R_S). Region IIIb is the perturbed, neutral environment region, pushed out by the outer shock (of radius R_n), which travels into the unperturbed environment (region IV).

We then remove this assumption, and derive a "thick HII region" model, which results in a differential equation which we integrate numerically. This model is described in § 4.

3. THIN HII REGION MODEL

3.1. *Derivation of the model equation*

As described in § 2, we assume that the stellar wind goes through a shock, and fills in a large bubble of hot, coronal gas. The kinetic energy of the wind feeds the thermal energy of the bubble and the kinetic energy of the swept-up material. The resulting energy equation is:

$$\frac{\dot{M} v_w^2}{2} t = \frac{3}{2} P V + \frac{1}{2} M_s v_s^2 \,, \qquad (1)$$

where $\dot{M}$ is the mass loss rate and v_w the terminal velocity of the wind, P and V are the pressure and volume (respectively) of the stellar wind bubble and M_s and v_s are the mass and velocity (respectively) of the swept-up shell.

Following the classical derivation (see Dyson 1977, and references therein), we use the estimates

$$P \approx \rho_0 \dot{R}^2 \,, \quad M_s \approx \frac{4\pi}{3} R^3 \rho_0 \,, \quad v_s \approx \dot{R} \,, \qquad (2)$$

where R is the outer radius of the hot bubble (so that $V = 4\pi R^3/3$).

Combining equations (1–2), we obtain an energy conservation equation of the form:

$$\frac{\dot{M}v_w^2}{2}t = \frac{8\pi}{3}R^3P \;\rightarrow\; P = \frac{3\dot{M}v_w^2 t}{16\pi R^3}\,, \qquad (3)$$

for a bubble of uniform pressure P and radius R at an evolutionary time t.

The relations in equation (2) are strictly valid for the case in which the swept-up material (regions IIIa and IIIb in Figure 1) forms a thin shell. However, we will apply equation (3) for the case in which region IIIb (of neutral swept-up gas, see Figure 1) is not thin. This is not likely to result in large errors because the thermal energy of the shell dominates over the kinetic energy of the shell by a factor of ≈3. Therefore, an incorrect estimate of the kinetic energy of the (no longer thin) shell does not introduce large errors in the energy equation.

We now follow Raga et al. (2012a), and assume that the outer shock (driven by the swept-up shell into the undisturbed environment) is isothermal, so that the postshock velocity $v_{\rm ps}$ and pressure $P_{\rm ps}$ are given by the isothermal Rankine-Hugoniot relations:

$$v_{\rm ps} = \frac{c_0^2}{v_n}\,, \qquad P_{\rm ps} = \rho_0 v_n^2\,, \qquad (4)$$

where v_n is the shock velocity and ρ_0 the ambient density. In the following, we set $P_{\rm ps} = P$ (where $P_{\rm ps}$ is the post-shock pressure, see equation 4 and P the pressure of the hot bubble, see equation 3).

Also, from the standard "shock pushed by a piston" problem, we have the relation

$$v_n = v_{\rm ps} + \dot{R}\,, \qquad (5)$$

where $\dot{R}$ is the velocity of the outer edge of the hot bubble.

Now, combining equations (3–5), we obtain the differential equation:

$$\frac{dr}{d\tau} = \left(\frac{\tau}{r^3}\right)^{1/2} - \left(\frac{r^3}{\tau}\right)^{1/2}\,, \qquad (6)$$

where $r = R/R_0$ (the dimensionless radius of the bubble) and $\tau = t/t_0$ (dimensionless time), with:

$$R_0 \equiv \sqrt{\frac{3\dot{M}v_w^2}{16\pi\rho_0 c_0^3}}\,, \quad t_0 \equiv \frac{R_0}{c_0}\,, \qquad (7)$$

where c_0 is the isothermal sound speed of the undisturbed environment.

Once a solution $r(\tau)$ to equation (6) has been found, the outer radius R_n of the perturbed, neutral environment (region IV of Figure 1) can be found by combining equations (4–5) to obtain

$$\frac{dr_n}{d\tau} = \left(\frac{\tau}{r^3}\right)^{1/2}\,, \qquad (8)$$

where $r_n = R_n/R_0$ and r comes from the previously obtained solution (of equation 6). Equation (8) can then be integrated to obtain the (dimensional) radius $R_n = R_0 r_n$ of the spherical shock travelling into the neutral environment.

For parameters appropriate for a high density, ultracompact HII powered by a main sequence O7 star we have

$$R_0 = 0.76\,{\rm pc}\left(\frac{\dot{M}}{5\times10^{-7}\;M_\odot\;{\rm yr}^{-1}}\right)^{1/2} \left(\frac{v_w}{2500\,{\rm km\,s^{-1}}}\right)\left(\frac{10^7\,{\rm cm^{-3}}}{n_0}\right)^{1/2}\left(\frac{1\,{\rm km\,s^{-1}}}{c_0}\right)^{3/2}\,, \qquad (9)$$

where n_0 is the number density of atomic nuclei. From this value of R_0 we can calculate the characteristic time $t_0 = R_0/c_0 \approx 7\times10^5$ yr. Therefore, ultracompact HII regions (with sizes of ∼0.1 pc and evolutionary times $\sim10^5$ yr) are in a regime with a dimensionless radius $r = R/R_0 \sim 0.1 - 1$ and a dimensionless time $\tau = t/t_0 \sim 0.1 - 1$.

3.2. *Numerical and analytic solutions*

Equation (6) can be integrated numerically with the initial condition $r(0) = 0$ to obtain the radius R of the hot bubble as a function of time, and an integration of equation (8) gives the radius R_n of the outer shock vs. t. The results of such integrations are shown in Figure 2.

It is possible to find a series of approximate analytic solutions to equation (6). For $\tau \ll 1$ the first term on the right hand side of equation (6) dominates over the second term, and (neglecting the second term) one then obtains the integral

$$r(\tau) = \left(\frac{5}{3}\right)^{2/5}\tau^{3/5}\,, \qquad (10)$$

which is the classical solution for an expanding, wind-driven bubble (see Dyson 1977).

For $\tau \gg 1$, the two terms on the right hand side of equation (6) become very large, reaching an approximate balance. Setting these two terms equal to each other, one obtains the solution

$$r(\tau) = \tau^{1/3}\,. \qquad (11)$$

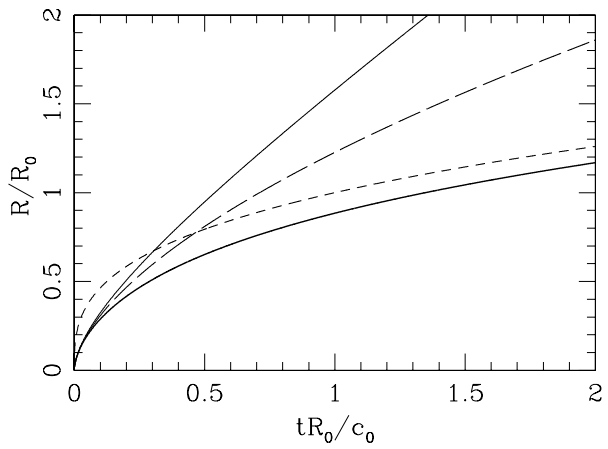

Fig. 2. Radius R of the thick shell (thick, solid line) and R_n of the outer shock (thin, solid line) resulting from a numerical integration of equations (6) and (8). The radii are given in units of R_0 (see equation 9) and the time in units of R_0/c_0 (where c_0 is the isothermal sound speed of the surrounding, neutral environment). The long-dash line shows the inner analytic solution (equation 10, valid for $R \ll R_0$) and the short-dash line the outer analytic solution (equation 11, valid for $R \gg R_0$).

It can be straightforwardly shown that this solution corresponds to a bubble in pressure equilibrium with the surrounding environment, expanding quasi-statically as more material is progressively injected by the stellar wind.

In Figure 2 we see that (as expected) the numerical integration of equation (6) gives a radius that approaches the low τ (equation 10) and high τ (equation 11) solutions in the appropriate limits. It is possible, however, to obtain approximate analytic solutions that reproduce the numerical solution for all values of τ.

To find these approximate solutions, we first rewrite equation (6) in the form:

$$\frac{dy}{dx} = \frac{3\left(x^2 - y^2\right)}{y^{2/3}}\,, \tag{12}$$

with $x = \tau^{1/2}$ and $y = r^{3/2}$. This equation can be straightforwardly solved to obtain x as a function of dx/dy and y, and the resulting relation can then be used to do successive iterations of the form:

$$x_{n+1} = \sqrt{y^2 + \frac{y^{2/3}}{3(dx_n/dy)}}\,, \tag{13}$$

to obtain increasingly more accurate approximations to the $y(x)$ solution of equation (12).

Let us call $x_0(y)$ the first approximation to the solution of equation (12). One possibility is to set $x_0(y)$ equal the large τ solution (equation 11), which in terms of the x, y variables takes the form

$$x_0(y) = y\,. \tag{14}$$

Inserting this relation in equation (13), we obtain the first iteration:

$$x_1(y) = \sqrt{y^2 + \frac{1}{3}y^{2/3}}\,. \tag{15}$$

Reinserting $x_1(y)$ in equation (13) we then obtain the second iteration:

$$x_2(y) = \sqrt{y^2 + \frac{3y\sqrt{y^2 + \frac{1}{3}y^{2/3}}}{1 + 9y^{4/3}}}\,. \tag{16}$$

It is possible to proceed with further iterations, but the resulting $x(y)$ relations are very extended.

A second possibility is to use the small τ solution (equation 10) as the first guess. The iterations then proceed as follows:

$$x_0(y) = \left(\frac{3}{5}\right)^{1/3} y^{5/9}\,, \tag{17}$$

$$x_1(y) = \sqrt{y^2 + \left(\frac{3}{5}\right)^{2/3} y^{10/9}}\,, \tag{18}$$

$$x_2(y) = \sqrt{y^2 + \frac{y^{2/3}\sqrt{y^2 + \left(\frac{3}{5}\right)^{2/3} y^{10/9}}}{3\left[y + \frac{1}{3}\left(\frac{5}{3}\right)^{1/3} y^{1/9}\right]}}\,. \tag{19}$$

The two "second iteration" solutions (equations 16 and 19) are shown (together with the results from a numerical integration of equation 6) in the top panel of Figure 3.

In order to evaluate the accuracy of our two "second iteration" solutions (equations 16 and 19), we first calculate the corresponding τ vs. r relations, and then calculate the relative error in the radius

$$\epsilon(\tau) = \left|\frac{r_e(\tau) - r_2(\tau)}{r_e(\tau)}\right|\,, \tag{20}$$

where $r_e(\tau)$ is the "exact" solution (obtained from a an accurate numerical integration of equation 6) and $r_2(\tau)$ is one of the two "second iteration" approximate solutions (equations 16 and 19).

The two corresponding relative errors are plotted as a function of time in the bottom panel of Figure 3. From this graph we see that the approximate solution given by equation (16) has a maximum deviation from the exact solution of $\sim$10%, and that the more complex approximate solution given by equation (19) has a maximum deviation of $\sim$5%.

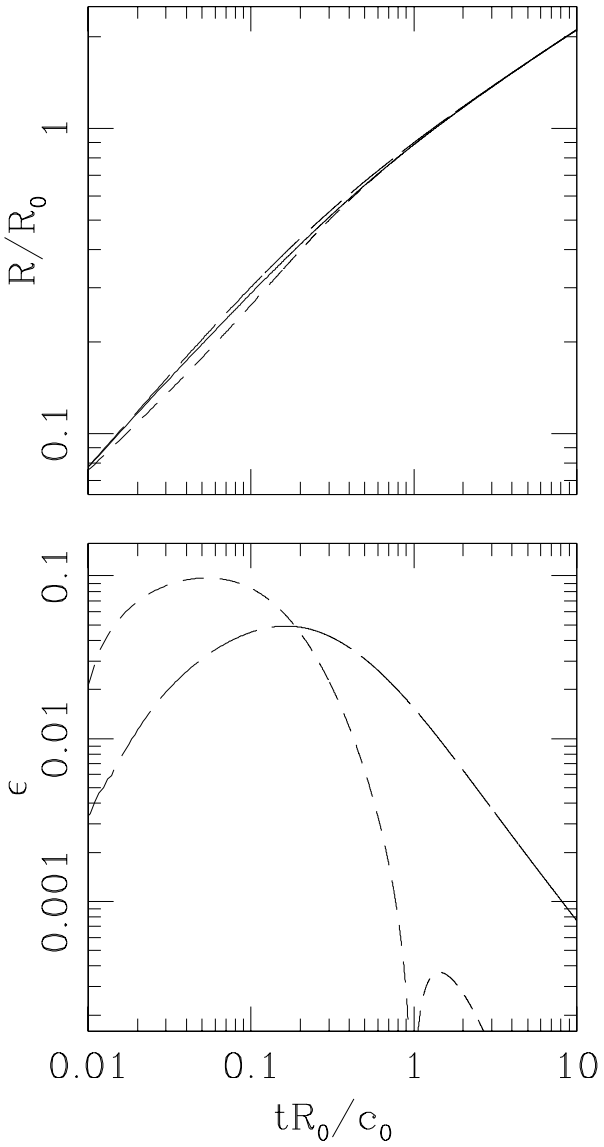

Fig. 3. Top panel: radius of the hot bubble as a function of time obtained from the "exact" (i.e., numerical) solution of equation 6 (solid line) and the radii obtained from the two approximate analytic solutions (short dash: equation 16; long dash: equation 19). Lower panel: relative deviations (see equation 20) of equation 16 (short dash) and equation 19 (long dash) from the "exact" solution.

4. THICK HII REGION MODEL

4.1. *Derivation of the model equation*

We now develop a model similar to that of § 3.1, but relaxing the condition that the photoionized region (region IIIa in Figure 1) is narrow. If we assume photoionization equilibrium (correct for all HII regions, as discussed in detail by Raga et al. 2012a), the outer radius R_S of the photoionized region obeys the relation:

$$S_* = \frac{4\pi}{3} n_i^2 \alpha_{\rm H} \left(R_S^3 - R^3\right) , \tag{21}$$

where R is the radius of the hot bubble (region II of Figure 1), n_i is the ion number density of region IIIa (assumed to be homogeneous within the region), S_* is the rate of photoionizing photons (emitted by the central star), $\alpha_{\rm H} \approx 2.6 \times 10^{-13}$ cm^3 s^{-1} is the case B hydrogen recombination coefficient at 10^4 K.

The condition of pressure equilibrium between the photoionized region and the hot bubble is

$$P = \overline{m} n_i c_i^2 , \tag{22}$$

where P is the pressure of the stellar wind bubble (see equation 3), c_i ($\approx$10 km s^{-1}) is the isothermal sound speed of the photoionized gas and $\overline{m}$ is the average mass per ion (= 1.3 m$_{\rm H}$ for a 90% H, 10% He gas, by number).

Also, the condition of pressure equilibrium between regions IIIa (the photoionized region) and IIIb (the shocked, neutral region) implies that

$$P = \rho_0 v_n^2 , \tag{23}$$

where we have used the isothermal shock jump conditions (equation 4). As described in § 3.1, v_n is the velocity of the outer shock driven into the undisturbed environment.

Finally, the "shock pushed by a piston" relation (equation 5) now takes the form:

$$v_n = v_{\rm ps} + \dot{R}_S = \frac{c_0^2}{v_n} + \dot{R}_S , \tag{24}$$

where $\dot{R}_S$ is the velocity of the outer edge of the photoionized region, and to obtain the second equality we have used equation (4).

Combining equations (3) and (21–24), we obtain a differential equation for R_S of the form:

$$\frac{1}{c_0}\frac{dR_S}{dt} = \sqrt{\frac{P}{\rho_0 c_0^2}} - \sqrt{\frac{\rho_0 c_0^2}{P}} , \tag{25}$$

where

$$\frac{P}{\rho_0 c_0^2} = \lambda \left(\frac{R_f}{c_0} t\right) \left(\frac{R_f}{R_S}\right)^3 + \sqrt{\left(\frac{R_f}{c_0}\lambda t\right)^2 \left(\frac{R_f}{R_S}\right)^6 + \left(\frac{R_f}{R_S}\right)^3} . \tag{26}$$

The solutions of equations (25–26) depend on the value of the dimensionless parameter

$$\lambda \equiv \frac{1}{2}\left(\frac{R_0}{R_f}\right)^2 , \tag{27}$$

where R_0 is given by equations (7, 9) and

$$R_f = \left(\frac{3S_*}{4\pi n_0^2 \alpha_H}\right)^{1/3} \left(\frac{c_i}{c_0}\right)^{4/3} . \qquad (28)$$

R_f is the final radius obtained by a "wind-less" HII region which has reached pressure equilibrium with a surrounding, homogeneous neutral environment (see, e.g., the book of Dyson & Williams 1980). For parameters appropriate for an ultracompact HII region powered by an O7 star, we have

$$\lambda = 290 \left(\frac{\dot{M}}{5\times10^{-7}\ M_\odot\ \mathrm{yr}^{-1}}\right)^{1/2} \left(\frac{v_w}{2500\,\mathrm{km\,s^{-1}}}\right)^2 \times \left(\frac{10^7\,\mathrm{cm^{-3}}}{n_0}\right)^{1/3} \left(\frac{10^{49}\,\mathrm{s^{-1}}}{S_*}\right)^{2/3} \times \left(\frac{1\,\mathrm{km\,s^{-1}}}{c_0}\right)^{1/3} \left(\frac{10\,\mathrm{km\,s^{-1}}}{c_i}\right)^{8/3} . \qquad (29)$$

It is straightforward to see that equations (25–26) have the following two limits:

1. For $\lambda \gg 1$, these equations become equation (6) of § 3.1, i.e., the model for a wind-driven shell with a negligibly thin HII region,

2. For $\lambda = 0$, these equations are identical to equation (8) of Raga et al. (2012a, who modeled the expansion of an HII region in the absence of a stellar wind).

Therefore, by spanning all positive values of the dimensionless parameter λ, we have models ranging from a "wind-less" to a "wind dominated" expanding HII region.

In the following section we present numerical solutions (of equations 25–26) giving the radius R_S of the expanding HII region as a function of time. We also integrate equation (8) (setting $r = R_S/c_0$ in the right hand term) to obtain the radius R_n if the outer shock driven into the undisturbed environment, and we combine equations (21–22) to obtain the radius of the hot bubble (region II of Figure 1):

$$\left(\frac{R}{R_f}\right)^3 = \left(\frac{R_S}{R_f}\right)^3 - \left(\frac{\rho_0 c_0^2}{P}\right)^2 , \qquad (30)$$

where the second term on the right is given by equation (26).

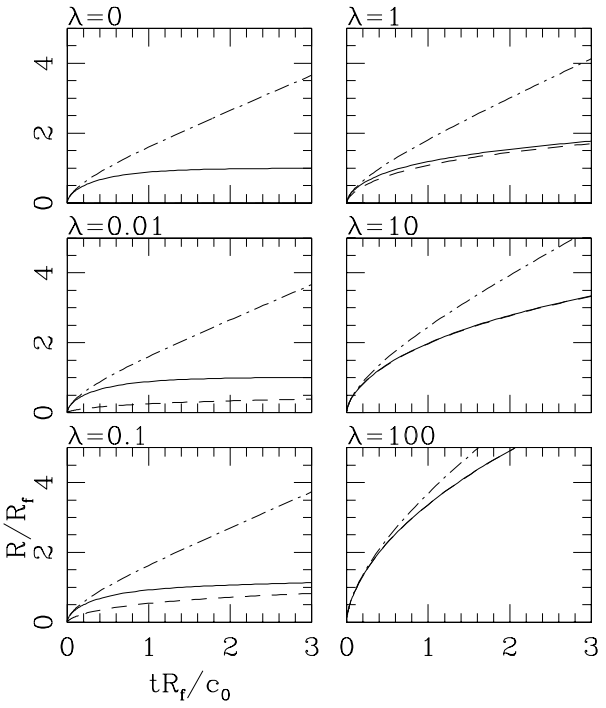

Fig. 4. Hot bubble radius (dashed line), outer radius of the HII region (solid line) and radius of the shock driven into the surrounding environment (dash-dotted line) as a function of time, obtained from numerical solutions of the "thick HII region model" of § 4. The six panels are labeled with the values of the dimensionless parameter λ (see equations 27, 29) used for each solution.

4.2. *Numerical solutions*

In Figure 4, we show the numerical results obtained from numerical integrations of the "thick HII region" model (described in § 4.1) for different values of the dimensionless parameter λ (see equations 27, 29). The $\lambda = 0$ solution (top left panel) is identical to the "wind-less expanding HII region" model of Raga et al. (2012a). The $\lambda = 100$ solution is most similar to the "thin HII region" model described in § 3 (i.e., the solution shown in Figure 2).

As can be seen in Figure 4, for progressively larger values of λ, a larger, inner hot wind bubble and a narrower HII region are obtained. In order to evaluate the relative thickness of the HII region, we have computed the value of

$$\frac{\Delta R}{R_S} = \frac{R_S - R}{R_S} , \qquad (31)$$

(where R_S and R are the outer radii of the HII region and of the hot bubble, respectively) as a function of t. The results are shown in Figure 5, in which we see that for $\lambda = 10$, the HII region has become a shell

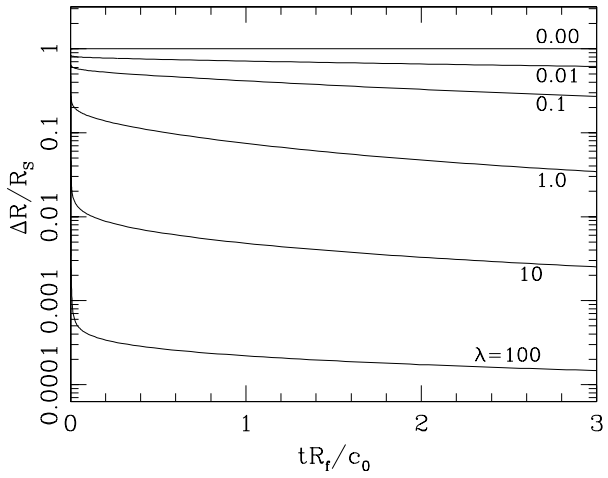

Fig. 5. Relative width of the HII region (see equation 31) as a function of time obtained for different values of the dimensionless parameter λ (see equation 27).

with a thickness of ∼1% of the radius of the ionized nebula. For the $\lambda \sim 100$ value expected for ultracompact HII regions driven by a main sequence O star (see equation 29), the photoionized gas is confined to an extremely narrow shell (see Figure 5).

5. SUMMARY AND DISCUSSION

In this paper, we have applied the "thick shell" formalism of Raga et al. (2012a, who modeled the expansion of an HII region photoionized by a wind-less source) to the case of a source producing both a photoionizing radiation field and a stellar wind. For the case in which the HII region is thin (compared to the width of the swept-up ambient medium shell), the problem can be solved analytically with an iterative method. This method gives solutions which approximate the exact solution with accuracies of better than ∼5% (see § 3.2). Our new solution to the wind-driven bubble expansion problem has a transition from a $R \propto t^{3/5}$ law (i.e., the "classical" solution, see Dyson 1977) for $R \ll R_0$ (see equation 9) to a $R \propto t^{1/3}$ law for $R \gg R_0$. Ultracompact HII regions lie close to the transition between these two regimes. Interestingly, this analytic solution has been missed in previous studies of wind-driven HII regions (see the review of Capriotti & Kozminski 2001).

The problem in which the HII region is not thin leads to a more complex differential equation, which we have integrated numerically (see §§ 4.1 and 4.2). Different solutions are found for different values of the dimensionless parameter $\lambda \equiv R_0/(2R_f)$ (where

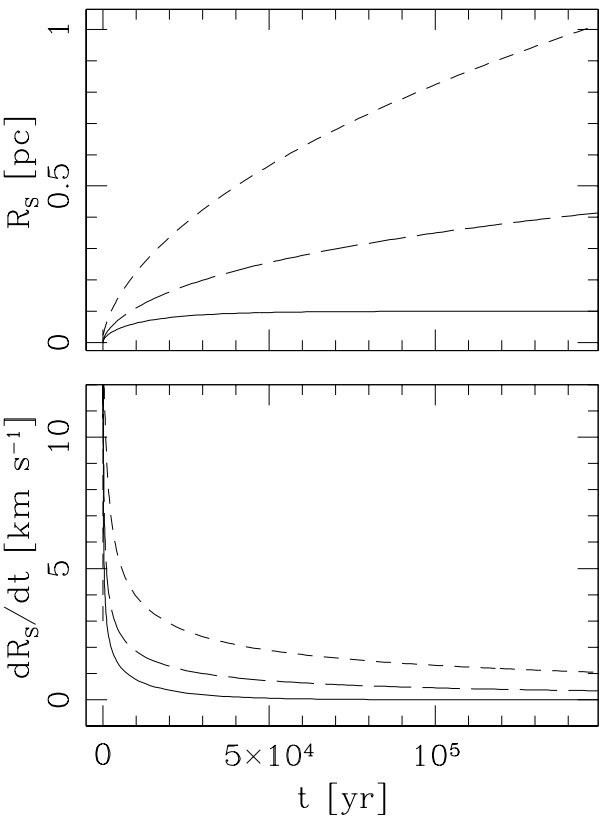

Fig. 6. Outer radius of the HII region (upper panel) and expansion velocity (lower panel) for an ultracompact HII region (of isothermal sound speed $c_i = 10$ km s^{-1}) driven by a source with $S_* = 10^{49}$ s^{-1} into a uniform environent of density $n_0 = 10^7$ cm^{-3} (and isothermal sound speed $c_0 = 1$ km s^{-1}). Three solutions are shown, corresponding to stellar winds such that the dimensionless parameter λ (see equations 27, 29) has values of 290 (short dash line), 10 (long dash line) and 0 (solid line).

R_0 is given by equation 9 and R_f is the final, pressure equilibrium radius of an HII region from a wind-less source). For increasing values of λ, we obtain solutions ranging from the wind-less case ($\lambda = 0$) to solutions in which the HII region becomes a very thin shell (approaching the "thin HII region" analytic solutions derived in § 3.2).

The transition to the thin HII region regime (for increasing λ values) is shown in Figures 4 and 5. Interestingly, for the nominal parameters that we have chosen for an ultracompact HII region, we obtain $\lambda \approx 300$ (see equation 29), so that they are clearly in the "thin HII region" regime.

In order to illustrate the effect of a stellar wind on the characteristics of an HII region, in Figure 6 we show the HII region radius R_S and the expan-

sion velocity (dR_S/dt) obtained for $\lambda = 0$ (i.e., a wind-less HII region), $\lambda = 290$ (the value obtained for our chosen ultracompact HII region parameters, see equation 29) and for $\lambda = 10$ (an arbitrary, intermediate λ value). From this Figure we see that while for $\lambda = 0$ the expansion velocity falls below $\approx$1 km s^{-1} in $\sim$500 yr, for $\lambda = 10$ the expansion velocity remains above $\approx$1 km s^{-1} for an evolutionary time $\sim 1.5\times10^5$ yr. For $\lambda = 290$, the expansion velocity remains above $\sim$3 km s^{-1} for $\sim 2\times10^4$ yr and above $\sim$2 km s^{-1} for $\sim 1.5\times10^5$ yr. Such expansion velocities might be detected (using the techniques of Kawamura & Masson 1998) in future interferometric observations with, e.g., MERLIN and the EVLA.

Interferometric observations show that some ultracompact HII regions have a "thick shell" morphology, with shell widths of $\sim$10–20% of the nebular radius (see Carral et al. 2002). Comparing this result with our predictions of the thickness of the HII region, we would conclude that these "thick shell" objects have a dimensionless parameter $\lambda < 1$ (see Figure 5).

However, from equation (29) and the table of main sequence O/B stellar parameters of Sternberg, Hoffman, & Pauldrach (2003), we see that HII regions (expanding into a $n_0 = 10^7$ cm^{-3}, uniform environment) have $\lambda = 150 \rightarrow 670$, the lower limit corresponding to a B0 star, and the upper limit to an O3 star. If we lower the environmental density to $n_0 = 10^4$ cm^{-3}, we would obtain a $\lambda = 15 \rightarrow 70$ range (see equation 29), still an order of magnitude larger than the λ values necessary for producing a "thick HII shell" morphology (see above and Figure 5).

As there are no empirical estimates of mass loss rates from main sequence stars later than B0.5 (see, e.g., Sternberg et al. 2003, and the review of Kudritzki & Puls 2000), it is not clear what are the values of λ for sources of later spectral type. If we use the $\dot{M} \approx 1.3 \times 10^{-11}\ M_\odot$ yr^{-1} mass loss rate for a B2 main sequence star ($T_{\rm eff} = 21000$ K, $\log_{10} g = 4$, see Strom & Peterson 1968) predicted by Babel (1996), a $v_w = 1000$ km s^{-1} wind velocity (see Figure 10 of Kudritski & Puls 2000) and $S_* = 2.9 \times 10^{44}$ s^{-1} (Díaz-Miller, Franco, & Shore 1998), we obtain $\lambda = 1.2$ for an HII region expanding into a $n_0 = 10^7$ cm^{-3} environment, and $\lambda = 0.12$ for $n_0 = 10^4$ cm^{-3}. Therefore, for a B2 central source we would indeed expect to have ultracompact HII regions with "thick shell" morphologies (see Figure 5).

Interestingly, the more recent paper of Marcolino et al. (2009) calculates mass loss rates for O8 and O9 main sequence which are two orders of magnitude below previously obtained rates (such as the ones of Sternberg et al. 2003, see above). These new mass loss rates would imply that $\lambda \sim 1$ for late OV stars.

Given the current lack of knowledge about winds from late O and early B main sequence stars, future comparisons between the models presented in this paper and observations of ultracompact HII regions might help to provide constraints on the values of the mass loss rates ($\dot{M}$) and terminal wind velocities (v_w) of these stars. However, comparisons between "thick shell" ultracompact HII regions and our quasi-analytic models are complicated by the fact that numerical simulations of wind-driven HII regions (see, e.g., García-Segura & Franco 1996) produce thin shells that can develop strong instabilities (a discussion of the physics of some of the instabilities of thin-shell HII regions is presented by Breitschwerdt & Kahn 1988, and Kahn & Breitschwerdt 1990). These instabilities lead to corrugations of a thin HII region which could result in an apparent "thick shell" morphology. Therefore, future attempts to derive wind properties from the intensities, sizes, expansion velocities and shell thicknesses of "thick shell" ultracompact HII regions will produce relatively uncertain results.

Regarding the model described above, the most important problem with it is that it does not include the inertia of the swept-up environment. Raga et al. (2012a) and Raga, Cantó, & Rodríguez (2012b) show that this inertia introduces important effects in the early evolution of the HII region expansion. However, there is no clear way of including this inertia in an analytic (or quasi-analytic) approach, so that the only way forward appears to be in the direction of full, numerical solutions to the 1D Euler equations (see Raga et al. 2012b). A second limitation is that the present model assumes that the radius of the stellar wind shock (i.e., the outer boundary of region I, see Figure 1) is negligibly small compared to the size of the HII region. This might not be the case in the early evolution of the system, for which a "working surface" description (see Kwok, Purton, & Fitzgerald 1978) might be more appropriate.

Finally, we would like to point out the recent paper of Arthur (2012), which presents results from numerical solutions of the full 1D Euler equations for basically the same problem that has been treated here. A detailed comparison between our quasi-analytic models and the simulations of Arthur (2012) should be made in the future in order to test their accuracy.

We acknowledge support from the Conacyt grants 61547, 101356 and 101975 and from DGAPA, Universidad Nacional Autónoma de México.

REFERENCES

Arthur, S. J. 2012, 2012, MNRAS, 421, 1283
Babel, J. 1996, A&A, 309, 867
Breitschwerdt, S., & Kahn, F. D. 1988, MNRAS, 235, 1011
Capriotti, E. R., & Kozminski, J. F. 2001, PASP, 113, 677
Carral, P., Kurtz, S. E., Rodríguez, L. F., Menten, K., Cantó, J., & Arceo, R. 2002, AJ, 123, 2574
de Pree, C. G., Rodríguez, L. F., & Goss, W. M. 1995, RevMexAA, 31, 39
Díaz-Miller, R. I., Franco, J., & Shore, S. N. 1998, ApJ, 501, 192
Dyson, J. E. 1977, A&A, 59, 161
Dyson, J. E., & de Vries, J. 1972, A&A, 20, 223
Dyson, J. E., & Williams, D. A. 1980, The Physics of the Interstellar Medium (Manchester: Manchester Univ. Press)
García-Segura, G., & Franco, J. 1996, ApJ, 469, 171
Falle, S. A. E. G. 1975, A&A, 43, 323
Franco, J., García-Segura, G., Kurtz, S. E., & Arthur, S. J. 2007, ApJ, 660, 1296
Kahn, F. D., & Breitschwerdt, S. 1990, MNRAS, 242, 209
Kawamura, J. H., & Masson, C. R. 1998, ApJ, 509, 270
Kudritzki, R. P., & Puls, J. 2000, ARA&A, 38, 613
Kurtz, S. 2005, in IAU Symp. 227, Massive Star Birth: A Crossroads of Astrophysics, ed. R. Cesaroni, M. Felli, E. Churchwell, & M. Walmsley (Cambridge: Cambridge Univ. Press), 111
Kwok, S., Purton, C. R., & Fitzgerald, P. M. 1978, ApJ, 219, L125
Marcolino, W. L. F., Bouret, J.-C., Martins, F., Hillier, D. J., Lanz, T., & Escolano, C. 2009, A&A, 498, 837
Pikel'ner, S. B. 1968, Astrophys. Lett., 2, 97
Raga, A. C., Cantó, J., & Rodríguez, L. F. 2012a, MNRAS, 419, L39
_____. 2012b, RevMexAA, 48, 149
Sternberg, A., Hoffman, T. L., & Pauldrach, A. W. A. 2003, ApJ, 599, 1333
Strom, S. E., & Peterson, D. M. 1968, ApJ, 152, 859

J. Cantó: Instituto de Astronomía, Universidad Nacional Autónoma de México, Apdo. Postal 70-242, 04510 México D. F., Mexico.
A. C. Raga: Instituto de Ciencias Nucleares, Universidad Nacional Autónoma de México, Apdo. Postal 70-543, 04510 México, D.F., Mexico (raga@nucleares.unam.mx).
L. F. Rodríguez: Centro de Radiostronomía y Astrofísica, Universidad Nacional Autónoma de México, Apdo. Postal 3-72 (Xangari), 58089 Morelia, Michoacán, Mexico (l.rodriguez@crya.unam.mx).